9 March 2001

ELSEVIER

Chemical Physics Letters 336 (2001) 81–87

CHEMICAL PHYSICS LETTERS

www.elsevier.nl/locate/cplett

Dissociative photodetachment of $SO_2 \cdot SO_2^-$: evidence for the S–O bound dimer

Runjun Li, Leah-Nani S. Alconcel, Robert E. Continetti *

Department of Chemistry and Biochemistry, University of California, San Diego, 9500 Gilman Drive, La Jolla, CA 92093-0340, USA

Received 20 October 2000

Abstract

Studies of the dynamics of the dissociative photodetachment of $(SO_2)_2^-$ reveal a strong preference in translational energy partitioning that can be related to the structure of $(SO_2)_2^-$ using a simple impulse model. An anisotropic product angular distribution was also observed, indicative of a rapid dissociation on a repulsive potential energy surface. Over a wide range of available energies the translational energy distributions for this DPD process peak at ≈36% of the available energy, consistent with the soft-bond impulse model prediction that 33% of the available energy would appear in translation for an OSO–SO_2 geometry (S–O bound) dimer anion.

1. Introduction

Polyatomic anions frequently form a variety of isomeric species [1]. Particularly when third row elements such as sulfur are involved, the complexity of the available structures increases markedly. The $(SO_2)_2^-$ dimer anion is an example of such a system, with three of the many possible geometries shown in Fig. 1. There have been a number of prior experimental studies of this dimer anion. These have included mass spectrometry [2–4], ion-beam studies of photodestruction, photodissociation, and photodetachment cross-sections [5–7] and, finally, photoelectron spectroscopy experiments by Bowen and co-workers [8] and more recently by Tsukuda et al. [9]. These studies have shown that this anion is stabilized relative to $SO_2 + SO_2^-$ by approximately 1 eV. The photoelectron spectra of $(SO_2)_2^-$ bear very little resemblance to the SO_2^- spectrum, showing that the electron is shared significantly between the two SO_2 moieties. Photodissociation studies by Bowers and co-workers [6] showed that ionic photodissociation competes strongly with photodetachment in the visible region of the spectrum (458–656 nm), and that dissociation occurs promptly on a repulsive ionic state, with anisotropic product angular distributions. Examination of the energy partitioning in these ionic photodissociation experiments [6] with a simple impulsive model of the dissociation dynamics provided tentative evidence for the O–O bound dimer (structure **1**) from among the possible structures shown in Fig. 1.

Motivated by the photofragmentation studies of Bowers and co-workers and the recent suggestions by Schwarz et al. [2] that different isomers of the anion can be prepared by varying ion source conditions, Berthe-Gaujac et al. have carried out ab initio calculations on isomeric forms of the SO_2 dimer anion [10,11]. These studies have identified

* Corresponding author. Fax: 1-619-534-7042.
E-mail address: rcontinetti@ucsd.edu (R.E. Continetti).

0009-2614/01/$ - see front matter
PII: S0009-2614(01)00033-1

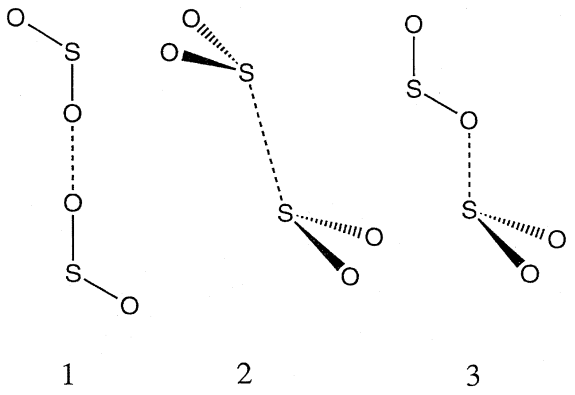

Fig. 1. A schematic view of several proposed structures for the $(SO_2)_2^-$ isomers.

at least two local minima on the anionic potential energy surface with energetics consistent with experimental observations. One involves the formation of a one-electron S–S bond between the two monomers [10] (structure **2** in Fig. 1) and the second one involves a two-electron S–O bond (structure **3** in Fig. 1) [11].

In this study, we have applied the technique of photoelectron–photofragment coincidence (PPC) spectroscopy to examine the dissociative photodetachment (DPD) of the sulfur dioxide dimer anion. DPD of negative ions occurs when photodetachment of the excess electron leaves the nascent neutral in a dissociative or predissociative state [12]. This process will even occur on the ground electronic state of the neutral system when the anion has an equilibrium geometry significantly different from the corresponding neutral. Franck–Condon photodetachment of the anion then leaves the neutral in a repulsive region of the potential energy surface leading to rapid dissociation. If the ensuing dissociation dynamics on the neutral surface are largely impulsive, insights into the precursor geometry can be gained, in addition to the energetics of the DPD process. To fully characterize such DPD processes, PPC experiments have proven to be a valuable method for understanding the energetic and dissociation dynamics of neutral and ionic species.

An important test of the nature of a photophysical process is an examination of the wavelength dependence of the translational energy release. Coincidence studies of the DPD of anions at a fixed photodetachment wavelength allow a similar study of the product translational energy as a function of excitation energy. Coincident measurement of the photoelectron kinetic energy fixes the total energy available to the neutral $(SO_2)_2$. Thus, at a given wavelength the distribution of photoelectron kinetic energies governs the distribution of energies available to product translation in the DPD process, providing information in a single experiment very similar to that accessible in photodissociation experiments carried out as a function of wavelengths such as the work by Kim and Bowers [6].

In the work presented in this Letter, we apply PPC spectroscopy to study the dissociative photodetachment of $(SO_2)_2^-$, and provide further experimental insights into possible equilibrium structures of the $(SO_2)_2^-$ dimer anion. In the following section we briefly review the experimental technique followed by a presentation and discussion of the experimental results. A striking trend in the observed partitioning of energy between the photoelectron and the photofragments can be interpreted in terms of an impulsive model for dissociation, consistent with the S–O bound dimer anion shown as structure **3** in Fig. 1.

2. Experimental

The photoelectron–photofragment coincidence spectrometer used in these experiments has been previously described in detail [13,14], so only a brief overview will be given here. Anions are produced in a 1 kHz pulsed free-jet expansion by electron impact on pure SO_2 with a 1 keV electron beam. In the free jet, anions at $m/e = 128$ are formed by secondary electron attachment processes and collisionally cooled in the expansion. The anions pass through a skimmer to enter a differentially pumped chamber where they are accelerated to energies of 3–4 keV and mass-selected by time-of-flight. The high beam energy is required for efficient detection of the neutral particles produced by photodetachment. In the interaction region the ion packet is intercepted orthogonally by the linearly polarized 100 ps pulsed output of a

tripled Nd:YAG laser operating at 355 nm [15]. The laser fluence used was ≈200 MW/cm^2.

The laboratory kinetic energy and recoil angle of photodetached electrons were determined by time-of-flight and position-of-arrival using a large-solid-angle photoelectron detector. This detector was centered above the intersection of the laser and ion beam, and subtended ≈4% of the full solid angle. The photoelectron recoil angle was measured to allow correction for the large Doppler shift produced by the fast ion beam, yielding the center-of-mass electron kinetic energy (*eKE*). The short laser pulse allowed accurate *eKE* measurements by time-of-flight with a nominal flight path of only 7.5 cm. Determination of the *eKE* fixes the energy remaining in the neutral complex. The center-of-mass electron kinetic energy resolution is ≈4% $\Delta E/E$, with an accuracy of ≈1.5% in this energy range determined by calibration experiments on the photodetachment with I^- and O^-.

If the neutral species dissociated, photofragments recoiled out of the beam and impinged on a two-particle time- and position-sensitive detector. Residual anions were removed from the beam with an electrostatic deflector, allowing only stable neutrals and neutral photofragments to reach the detector. Conservation of linear momentum in the center-of-mass frame determined the mass ratio of the coincident photofragments. Given the mass ratio, beam velocity, flight path and the time and position of photofragment arrival, the center-of-mass translational energy, E_T, and the product recoil angles in the center-of-mass frame were determined [16]. To be detected photofragments had to clear a beam-block of 7 mm diameter centered on the detector. This beam block was required to prevent photofragments from one half of the detector paralyzing the other half, giving a low-energy E_T cutoff in the data acquisition producing equal mass photofragments of 10 meV at the lower beam energy of 3 keV. Counting statistics provide an estimate for false coincidences in this experiment of ≈4%. The resolution of the E_T measurement is ≈10% $\Delta E_T/E_T$ and the accuracy is ≈2% [13].

Measurement of the translational energy release between the photofragments in coincidence with the photoelectron kinetic energy provides a direct measure of the partitioning of kinetic energy in the system, yielding a complete kinematic characterization of dissociative photodetachment events producing an electron and two neutral photofragments. Ionic photodissociation processes yielding stable ionic photofragments were observed by turning off the electrostatic deflection field and recording ionic and neutral photofragments. Ionic photodissociation was seen to occur as a minor channel consistent with the earlier work of Kim and Bowers [6].

3. Results

The photoelectron–photofragment kinetic energy correlation spectrum, $N(E_T, eKE)$, provides the most complete view of the energy partitioning observed in this study. This is a two-dimensional histogram revealing directly the correlation between events characterized by specific *eKE* and E_T values. The correlation spectrum is represented by a contour map as shown in Fig. 2. At the left of the contour map is shown the $N(eKE)$ spectrum, obtained by integrating the spectrum over E_T. The peak in the $N(eKE)$ distributions shows that the vertical detachment energy (VDE) is 2.77 eV, in good accord with the photoelectron spectroscopy measurements of Tsukuda et al. [9]. The $N(E_T)$ spectrum shown at the bottom is similarly obtained by integrating over *eKE*. The diagonal line located at 1.47 eV in the contour map represents the total available energy, which can be calculated by

$$E_{AVL} = h\nu - D_0(SO_2\text{–}SO_2^-) - EA(SO_2) + E_{INT}(SO_2)_2^-. \quad (1)$$

Here, $h\nu$ is the photon energy (3.49 eV for 355 nm), $E_{INT}(SO_2)_2^-$ is the internal energy in the $(SO_2)_2^-$ cluster, $EA(SO_2)$ is the electron affinity of SO_2 ($EA = 1.11$ eV) [17] and $D_0(SO_2\text{–}SO_2^-)$ is the bond dissociation energy for $(SO_2)_2^- \rightarrow SO_2 + SO_2^-$. $E_{INT}(SO_2)_2^-$ is assumed to be negligible in our experiments, since the dimer ion $(SO_2)_2^-$ is formed by electron attachment in a free-jet expansion. This is the best measure for the maximum energy

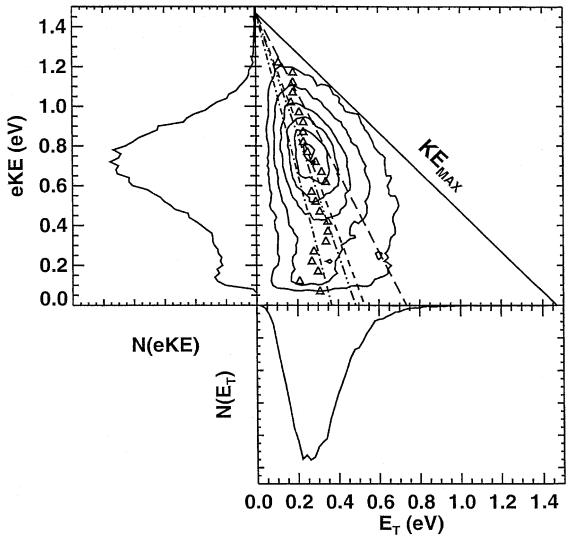

Fig. 2. $N(E_T, eKE)$ correlation spectrum recorded at 355 nm. The assigned maximum kinetic energy for the photoelectron + photofragments, $KE_{MAX} = 1.47$ eV, is shown as the solid diagonal line. The lowest contour, near KE_{MAX}, is at 4% of the peak, with the rest of the contours linearly spaced from 15% to 95%. The short dashed line shows the observed trend in the peak $N(E_T)$ spectra, while the dot-dashed, dot-dot-dashed and long-dashed lines are the expected positions for the fraction of the available energy released in the dissociation of the O–O (25%,), S–O (33%) and S–S (50%) bonds, respectively. The triangles denote the actual peak E_T as a function of eKE as discussed in the text.

appearing in translation (KE_{MAX}, either in the photoelectron or between the photofragments) in the present experiment. The bond dissociation energy (assumed to be at 0 K) $D_0(SO_2–SO_2^-) = 0.91 \pm 0.05$ eV obtained from Eq. (1) is in good accord with the previously measured 298 K bond dissociation enthalpies of 1.04 [18] and 0.92 eV [19]. This is an upper limit to the bond dissociation energy since the dynamics may lead to no ground-state SO_2 products.

The products of photodissociation are not generally isotropically distributed. A polarized laser beam is employed in our experiments. The probability for photon absorption is related to the projection of the electronic transition dipole moment of the molecule on the electric vector of the laser beam. Therefore, certain orientations of the cluster ions $(SO_2)_2^-$ within the ion beam selectively absorb photons. If the lifetime of the intermediate state excited by a photon is short relative to a rotational period then the photoproducts reflect more clearly their initial orientation on photon absorption than if the lifetime is comparable to a rotational period or larger. The anisotropic distribution of the photofragments is generally described by the equation [20]

$$P(\theta) = (4\pi)^{-1}[1 + \beta P_2(\cos\theta)]. \quad (2)$$

In Eq. (2), $P(\theta)$ is the probability per unit solid angle that the products recoil at an angle θ with respect to the electric vector of the photon, $P_2(\cos\theta)$ is the second associated Legendre polynomial in $\cos\theta$, and β is the anisotropy parameter characterizing the product angular distribution.

The velocities and recoil angles of the SO_2 photofragments are directly measured in this experiment, so it is straightforward to determine the center-of-mass photofragment angular distribution. In doing so, however, it is essential to correct for the fact that the detector does not accept all possible ranges of velocity and angle space due to the presence of the beam-block described above. Thus, a correction for the detector acceptance function is required to obtain the true center-of-mass photofragment energy and angular distributions as previously discussed [16,21]. The product translational energy distribution, $P(E_T)$, and the translational energy dependence of the photofragment anisotropy parameter, $\beta(E_T)$, found by this treatment are shown in Fig. 3. As the figure shows, $\beta \approx 0.7$ describes the photofragment angular distribution over a wide range of E_T, indicating that the transition moment for DPD is aligned along the photofragment recoil axis. As Fig. 3 shows, at $E_T < 0.13$ eV, the finite detector acceptance begins to have significant impact on the shape of the $P(E_T)$. No evidence was observed for stable products or a $P(E_T)$ actually peaking at $E_T = 0$ eV in separate product time-of-flight experiments with the beam-block removed, however. The peak position for the integrated $P(E_T)$ at $E_T = 0.225$ eV is not significantly affected by the detector acceptance function. This $P(E_T)$ distribution peaking away from zero is indicative of dissociation on a repulsive surface or over an exit channel barrier.

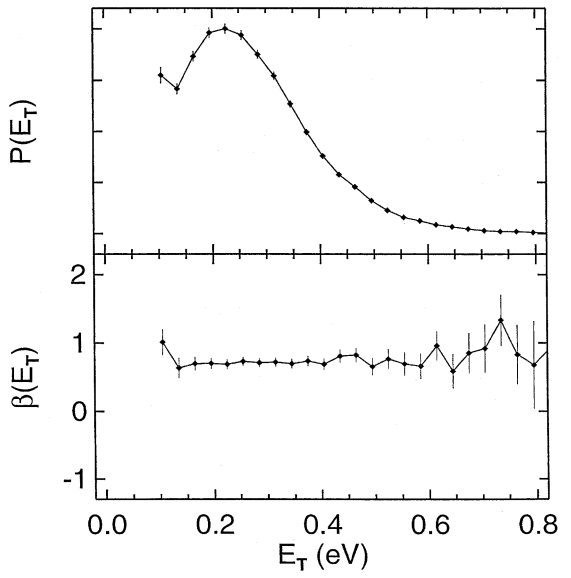

Fig. 3. Product translational energy, $P(E_T)$, and angular distributions, $\beta(E_T)$, for the DPD of $(SO_2)_2^-$ at 355 nm after correction for the detector acceptance function.

4. Discussion

Examination of the shape of the contours in the $N(E_T, eKE)$ spectrum reveals a striking trend in the observed peak in the product translational energy partitioning, E_T^{pk}. This trend is highlighted by the dashed line in Fig. 2 drawn along the locus where 36% of the available energy appears in translation of the photofragments. Subtracting the *eKE* from the total available energy, E_{AVL}, gives the energy available for translational and internal excitation of the SO_2 photofragments ($E_{AVL}^{SO_2}$). The dashed line in Fig. 2 shows a clear trend for the peak in the $N(E_T)$ distribution at 36% of $E_{AVL}^{SO_2}$ over a wide range of electron kinetic energies. This percentage is largely independent of E_{AVL}, as shown by the position of E_T^{pk} as a function of *eKE* plotted as triangles on the contour map of Fig. 2. These values were obtained from the $N(E_T)$ distributions obtained by integrating 0.05 eV-wide slices of the $N(eKE)$ spectrum, beginning at 0 eV.

As discussed in Section 1, theoretical calculations have predicted several isomers of $(SO_2)_2^-$, with the singly bound dimers including those with S–S, S–O and O–O intermolecular bonds [10,11]. The observation that the product translational energy peaks away from zero and the significant photofragment anisotropy characterized by $\beta = 0.7$ both indicate that the DPD of $(SO_2)_2^- + h\nu \rightarrow SO_2 + SO_2 + e^-$ occurs promptly on a repulsive surface, so it is interesting to examine the observed partitioning of energy in terms of an impulsive dissociation. The impulsive model, assuming a soft-bond between the atoms involved in the dissociating bond and the rest of the molecular fragments [6,22], predicts that the product translational energy should be a linear function of the energy available:

$$E_T = (\mu_{BC}/\mu_f)E_{AVL}^{SO_2}. \quad (3)$$

In Eq. (3), μ_{BC} is the reduced mass of the two atoms involved in the bond being broken and μ_f is the reduced mass of the fragments. Eq. (3) indicates that E_T should vary linearly with $E_{AVL}^{SO_2}$, which is in good agreement with the experimental distribution. While it is customary to examine the average fraction of the available energy appearing in translation, $f_T = \langle E_T \rangle / E_{AVL}^{SO_2}$, due to the detector cutoff at low E_T in the present experiment we examine the peak of the translational energy distribution, E_T^{pk}, as a function of available energy. In this regard, we note that the position of the peak is not affected by the detector acceptance function shown in Fig. 3, while $\langle E_T \rangle$ would be. The deviations of E_T^{pk} values, shown as the triangles plotted in Fig. 2, from the impulse model prediction at low and high $E_{AVL}^{SO_2}$ (high and low *eKE*, respectively) can be rationalized in terms of breakdown of the impulsive model. At very low $E_{AVL}^{SO_2}$, the assumption of an impulsive transfer of energy from the (slowly) breaking bond to the rest of the molecule is expected to break down, while at high $E_{AVL}^{SO_2}$, increased vibrational and rotational excitation in the SO_2 products may become possible.

Using the impulsive model, the various isomers of $(SO_2)_2^-$ are expected to yield very different results. In particular, O–O bond fission is expected to yield $E_T/E_{AVL} = 0.25$, S–O bond fission $E_T/E_{AVL} = 0.33$, and S–S bond fission, $E_T/E_{AVL} = 0.50$. These trend lines are also shown in Fig. 2. The observed propensity for $E_T^{pk}/E_{AVL}^{SO_2} \approx 0.36$ is most consistent with the involvement of an S–O bond in the dissociation step. The structure of the

$(SO_2)_2^-$ dimer involving one S–O bond was investigated by Berthe-Gaujac et al. [11], using ab initio calculations at the PUMP4/6-31+G*//UMP2/6-31+G* level. They found two nearly isoenergetic minima with one S–O bond. Both of these structures are such that an impulsive dissociation of the dimer would be expected to produce a torque on the recoiling products, leading to significant rotational excitation. This, and the relatively low vibrational frequencies in the SO_2 products, explains why no vibrational structure is observed in the correlation spectrum and the total kinetic energy distribution. The striking experimental result of $E_T^{pk}/E_{AVL} = 0.36$ is thus consistent with formation of the S–O bound dimer in our ion source. This conclusion is at variance with the qualitative analysis of the photoelectron spectra recorded by Tsukuda et al. [9] in terms of an S–S bound dimer. Given the difficulty associated with making structural conclusions from only the broad, dissociative photoelectron spectra and the striking nature of the observed energy partitioning in DPD, the present results provide an important new insight into the bonding in this dimer anion.

A schematic reaction coordinate diagram showing the processes and energies of interest is given in Fig. 4. The electron affinity of SO_2 and the binding energy of the neutral $(SO_2)_2$ dimer are from the literature [17,23]. The bond dissociation energy of $(SO_2)_2^-$, $D_0 = 0.91$ eV, is from this work. Like the previously studied O_4/O_4^- system [24], we assume that the anion is more tightly bound than the neutral dimer, so when the electron is removed the neutral dimer is located in a repulsive region of the surface. Thus, there is no Franck–Condon overlap with the 0.19 eV-deep van der Waals minimum on the neutral surface and no stable neutral dimers are produced by photodetachment.

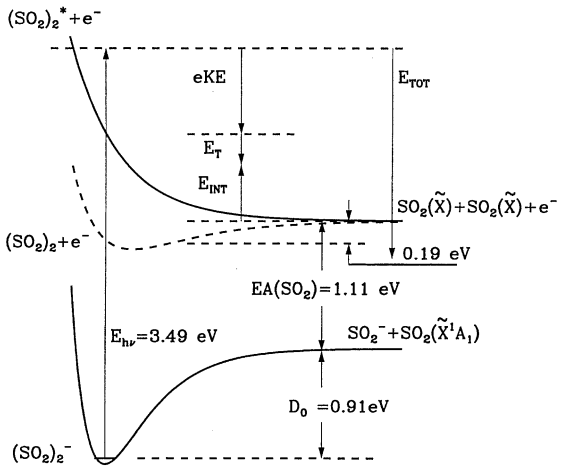

Fig. 4. Schematic energy diagram for the DPD of $(SO_2)_2^-$ at 355 nm, including as a dashed curve with a binding energy of 0.19 eV the neutral $(SO_2)_2$ system which is not in the Franck–Condon region for photodetachment.

It is interesting to consider the origin of the strongly anisotropic fragment angular distribution observed in the DPD of $(SO_2)_2^-$. If the departure of the electron and dissociation of the molecular species all happen on the time scale of a molecular vibration, then DPD is inherently a three-body process. An example of such a process is the DPD of O_4^- previously studied in this laboratory [25]. Theoretical treatments of photoionization have shown how to interpret the alignment produced in these processes in terms of the angular momentum transfer between the photoelectron and the molecular core [26,27]. DPD of a negative ion is analogous to dissociative photoionization, with the exception that the exit-channel interaction between the electron and the neutral complex occurs over a much shorter range than the Coulomb potential operative in photoionization. In particular, this means that alignment of the neutral molecule produced by photodetachment will depend on the partial wave composition of the electron continuum. The alignment observed is determined by the symmetry of both the initial (anion) state and the final (electron plus neutral) compound state. In future experiments we hope to measure the molecular-frame photoelectron angular distribution for this DPD process, which should provide further insights into the nature of the bonding in this dimer anion.

5. Conclusion

The dissociative photodetachment of $(SO_2)_2^-$ has been investigated at 355 nm. From the data we conclude the following. Dissociation occurs on a repulsive region of the potential energy surface for

ground state $(SO_2)_2$. The striking partitioning of translational energy, with the trend for the peak value for the translational energy release at 36% of the available energy appearing in translational degrees of freedom, is consistent with breaking an S–O bond between the two SO_2 moieties such as structure **3** in Fig. 1. These results also provide a new experimental value for the bond dissociation energy of the anionic dimer $D_0((SO_2)_2^-) = 0.91 \pm 0.05$ eV. Furthermore, the anisotropic product angular distribution indicates that the neutral dimer produced by photodetachment of the $(SO_2)_2^-$ undergoes a rapid dissociation.

Acknowledgements

This work was supported by the Chemistry Division of the National Science Foundation under grant CHE 97-00142. R.E.C. is a Camille Dreyfus Teacher–Scholar, and Alfred P. Sloan Research Fellow and a Packard Fellow in Science and Engineering. L.S.A. acknowledges the support of a Cota Robles Fellowship.

References

[1] M.S. Resat, V. Zengin, M.C. Garner, R.E. Continetti, J. Phys. Chem. A 102 (1998) 1719.
[2] M. Iraqi, N. Goldberg, H. Schwarz, Int. J. Mass Spectrom. Ion Process. 130 (1994) 127.
[3] A. Stamatovic, P. Scheier, T.D. Märk, Z. Phys. D 6 (1987) 351.
[4] A. Stamatovic, P. Scheier, T.D. Märk, Chem. Phys. Lett. 136 (1987) 177.
[5] R.V. Hodges, J.A. Vanderhoff, J. Chem. Phys. 72 (1980) 3517.
[6] H. Kim, M.T. Bowers, J. Chem. Phys. 85 (1986) 2718.
[7] T. Dresch, H. Kramer, Y. Thurner, R. Weber, Chem. Phys. Lett. 177 (1991) 383.
[8] J.T. Snodgrass, J.V. Coe, C.B. Freidhoff, K.M. McHugh, K.H. Bowen, J. Chem. Phys. 88 (1988) 8014.
[9] T. Tsukuda, T. Hirose, T. Nagata, Int. J. Mass Spectrom. Ion Process. 171 (1997) 273.
[10] N. Berthe-Gaujac, I. Demachy, Y. Jean, F. Volatron, Chem. Phys. Lett. 221 (1994) 145.
[11] N. Berthe-Gaujac, Y. Jean, F. Volatron, Chem. Phys. Lett. 243 (1995) 165.
[12] R.E. Continetti, Int. Rev. Phys. Chem 17 (1998) 227.
[13] C.R. Sherwood, K.A. Hanold, M.C. Garner, K.M. Strong, R.E. Continetti, J. Chem. Phys. 105 (1996) 10803.
[14] K.A. Hanold, C.R. Sherwood, M.C. Garner, R.E. Continetti, Rev. Sci. Instrum. 66 (1995) 5507.
[15] X. Xie, J.D. Simon, Opt. Commun. 69 (1989) 303.
[16] R.E. Continetti, in: Photoionization and Photodetachment, in: C.Y. Ng (Ed.), Advanced Series in Physical Chemistry, vol. 10B, World Scientific, Singapore, 2000, p. 748.
[17] M.R. Nimlos, G.B. Ellison, J. Phys. Chem. 90 (1986) 2574.
[18] R.G. Keesee, N. Lee, A.W. Castleman Jr., J. Chem. Phys. 73 (1980) 2195.
[19] J.R. Vacher, E. Le Duc, M. Fitaire, Int. J. Mass Spectrom. Ion Process. 135 (1994) 139.
[20] R.N. Zare, Mol. Photochem. 4 (1972) 1.
[21] C.R. Sherwood, R.E. Continetti, Chem. Phys. Lett. 258 (1996) 171.
[22] G.E. Busch, K.R. Wilson, J. Chem. Phys. 56 (1972) 3626.
[23] U.J. Breen, K. Kilgare, K. Stephan, R. Hofmann-Sievert, B.D. Kay, R.G. Keesee, T.D. Mark, A.W. Castleman Jr., Chem. Phys. 91 (1984) 305.
[24] K.A. Hanold, R.E. Continetti, Chem. Phys. 239 (1998) 493.
[25] K.A. Hanold, M.C. Garner, R.E. Continetti, Phys. Rev. Lett. 77 (1996) 3335.
[26] D. Dill, J. Chem. Phys. 65 (1976) 1130.
[27] C.H. Greene, R.N. Zare, Ann. Rev. Phys. Chem. 33 (1982) 119.